INTERNATIONAL JOURNAL FOR NUMERICAL METHOD IN ENGINEERING, VOL. 39, 469–488 (1996)

FINITE ELEMENTS FOR THREE-MODE INTERACTION IN BUCKLING ANALYSIS

EVER J. BARBERO*

Mechanical and Aerospace Engineering, Constructed Facilities Center, West Virginia University, Morgantown, WV 26506-6101, U.S.A.

LUIS A. GODOY†

Department of Civil Engineering, University of Puerto Rico, Mayaguez, Puerto Rico

IOANNIS G. RAFTOYIANNIS‡

Mechanical and Aerospace Engineering, Constructed Facilities Center, West Virginia University, Morgantown, WV 26506-6101, U.S.A.

SUMMARY

This paper presents a finite element formulation for the buckling mode interaction analysis of structures modelled as plate assemblies. The main assumptions are linear elasticity, a linear fundamental path, the existence of distinct critical states that are coincident or near coincident, and a coupled path arising from a linear combination of modal displacements due to interaction. The formulation adopted is known as the W-formulation, in which the energy is written in terms of a sliding set of incremental co-ordinates measured with respect to the fundamental path. The energy is then expressed with respect to a reduced modal co-ordinate basis and the coupled solution arising from interaction is computed. An example of a fibre-reinforced composite I-beam subjected to axial compression illustrates the procedure. The results are compared to a simplified model developed by the authors. Also, an imperfection sensitivity analysis is performed.

KEY WORDS: post buckling; interaction; composite materials

1. INTRODUCTION

Structural beams and columns formed by thin-walled elements display complex forms of buckling. Flanges may buckle locally and the column may buckle globally at loads that are close or even coincident. Coincidence of buckling loads may be due to particular operating conditions or the result of structural optimization.[1,2] When two or more modes of buckling correspond to loads that are close or coincident, interaction between the modes may lead to post-buckling behaviour quite different from the post-buckling behaviour of the participating modes. This has been observed for shells, thin-walled columns made of both isotropic materials[3] and fibre-reinforced composite materials.[4] In the latter paper, the authors present experimental results of buckling strength of I-columns up to 30 per cent lower than single-mode (local or Euler)

* Associate Professor
† Professor
‡ Graduate Research Assistant

0029–5981/96/030469–20

Received 22 February 1994
Revised 18 April 1995

predictions. From experimental observations, they conclude that the observed reduction is caused by modal interaction. Numerical results presented here show that modal interaction occurs, and that imperfection sensitivity of the column buckling load is only noticed when modal interaction is included.

In this work, it is assumed that the material behaves linearly until buckling occurs and during the initial stages of post-buckling. This has been documented experimentally for fibre-reinforced composite columns by Barbero and Tomblin[4] and Vakiener *et. al.*,[5] and for lateral-distortional buckling of beams by Mottram,[6] etc. Therefore, the general theory of elastic stability for discrete systems[7] constitutes an appropriate framework for the study of post-buckling behaviour with the aid of finite element discretization. Such a theory provides a similar understanding of critical loads as those obtained by Euler and Timoshenko, but it differs in that the general theory allows to study post-critical states, also accounting for imperfection sensitivity of the critical loads. This approach has been used by Flores and Godoy[8] for post-buckling analysis of shells of revolution showing isolated mode behaviour.

The determination of critical loads by eigenvalue analysis as well as the study of limit point behaviour using continuation methods, in the context of finite element discretizations, are common practice today. In this work, perturbation techniques are used to classify the nature of the bifurcation points and to follow the initial post-buckling path. Furthermore, interaction between three modes emerging from bifurcation points, two of which are close or coincident, is studied to identify tertiary paths emerging from the secondary paths. The tertiary paths may be quite different from the secondary paths identified by an isolated mode analysis, thus revealing a different kind of imperfection sensitivity of the structure.

The literature on mode interaction in discrete systems includes the works of Chilver,[9] Chilver and Jones,[10] Thompson and Supple,[11] Swanson and Croll,[12] Walker,[13] Reis,[14] Reis and Roorda,[15,16] Maaskant,[17] and Maaskant and Roorda.[18] Special problems that may arise while using continuation methods, as identified by Supple,[19] have motivated the use of perturbation techniques. The finite strip method was used by Graves Smith and Sridharan,[20] Sridharan and Graves Smith,[21] Benito and Sridharan,[22,23] Sridharan and Ali,[24,25] Sridharan and Peng,[26] and Mollmann and Goltermann,[27] while finite elements were used by Casciaro *et. al.*[28]

The finite element method was chosen in our work because of its superior versatility to model complex boundary conditions and because it automatically accounts for the problem of wave modulation.[29] Analytical methods were used by Koiter and Pignataro[30] for stiffened panels and by Kolakowski[31–33] to study trapezoidal columns. Applications of mode interaction analysis to fibre-reinforced composite structures can be found in the work of Stoll[34] and Sridharan and Starnes.[35] Since we are primarily interested in applications to fibre reinforced composite columns, a shear deformable finite element is used to model the structure as an assembly of plate elements.

2. EQUILIBRIUM PATH IN MODAL SPACE

The total potential energy V of a discrete or discretized system is a non-linear functional that may be written in terms of the generalized co-ordinates of the system denoted here by Q_i (usually nodal displacements). If the strain–displacement relations of the problem are assumed to be quadratic (the strains depend of the square of displacements), then the energy V results quadratic in Q_i. Following Croll and Walker,[36] it is convenient to split the energy V into terms that are constant, linear, quadratic, etc., in the displacements Q_i. This leads to an expression of the form (Reference 36 equation (7.38)).

$$V = \Lambda \hat{V}'_0 + \hat{V}_i Q_i + \tfrac{1}{2}\hat{V}_{ij} Q_i Q_j + \tfrac{1}{6}\hat{V}_{ijk} Q_i Q_j Q_k + \tfrac{1}{24}\hat{V}_{ijkl} Q_i Q_j Q_k Q_l \tag{1}$$

where $i, j, k, l = 1, \ldots, N$, N being the number of degrees of freedom of the system. The V'_0, V_i, V_{ij}, etc., are the coefficients in equation (1), but it can be shown that they are also the derivatives of V with respect to Q_i evaluated at the equilibrium state. Thus, equation (1) can be interpreted as a Taylor expansion of V in terms of Q_i. The nodal displacements can be written as

$$Q_i = \Lambda Q_i^{\mathrm{F}} + q_i \tag{2}$$

where q_i are the incremental displacements and Q_i^{F} is the response in the linear fundamental path for unit value of the load parameter Λ. Introduction of equation (2) into equation (1) results in the so-called W-energy which, after neglecting terms independent of q_i and terms with non-linear contribution from Q_i^{F}, can be written (see Reference 36, equation (7.86)) as

$$W = \hat{W}_i q_i + \tfrac{1}{2}\hat{W}_{ij} q_i q_j + \tfrac{1}{6}\hat{W}_{ijkl} q_i q_j q_k + \tfrac{1}{24}\hat{W}_{ijkl} q_i q_j q_k q_l \tag{3}$$

where

$$\begin{aligned} \hat{W}_i &= \hat{V}_i, & \hat{W}_{ij} &= \hat{V}_{ij} + \Lambda \hat{V}_{ijk} Q_k^{\mathrm{F}} \\ \hat{W}_{ijk} &= \hat{V}_{ijk} + \Lambda \hat{V}_{ijkl} Q_l^{\mathrm{F}}, & \hat{W}_{ijkl} &= \hat{V}_{ijkl} \end{aligned} \tag{4}$$

The same approach (W-formulation) has been used in the same context (finite elements) by Mau and Gallagher[37] and Gallagher.[38] For a critical state, we are interested in following the post-buckling path using perturbation techniques. We select a suitable generalized co-ordinate as perturbation parameter (say q_1) and we express the load Λ and the remaining generalized co-ordinates q_i ($i \neq 1$) as

$$\begin{aligned} \Lambda &= \Lambda^{\mathrm{C}} + \Lambda^{(1)\mathrm{C}} q_1 + \tfrac{1}{2}\Lambda^{(2)\mathrm{C}} q_1^2 + \cdots \\ q_i &= q_i^{(1)\mathrm{C}} q_1 + \tfrac{1}{2} q_i^{(2)\mathrm{C}} q_1^2 + \cdots \end{aligned} \tag{5}$$

where superscripts (1)C and (2)C are first- and second-order derivatives with respect to the perturbation parameter q_1, evaluated at the critical state. The condition of critical stability state is

$$[\hat{V}_{ij} + \Lambda \hat{V}_{ijk} Q_k^{\mathrm{F}}] x_j = 0 \tag{6}$$

The solution of equation (6) is a set of N eigenvalues, which we will denote as Λ^n (the superscript will identify the mode to which we are referring), and eigenvectors $\mathbf{x}^n$, for $n = 1, \ldots, N$. These modes are orthogonal to each other, so that

$$x_j^n \cdot x_j^m = 0, \quad n \neq m \tag{7}$$

but they also satisfy

$$[\hat{V}_{ijk} Q_k^{\mathrm{F}}] x_j^m x_i^n = \delta_{mn} \tag{8}$$

We next assume that there is a set of three eigenvalues with two of them being relatively close, or even coincident. We will refer to these three eigenvalues Λ^n (for $n = 1, 2, 3$) as active, in the sense that they play a crucial role in the interactive buckling process. The remaining $N - 3$ eigenvalues (for $n = 4, \ldots, N$) are *passive* and they play no role in the analysis.

As an approximation, we could think of a linear combination of the three modes that may be sufficient to reflect mode interaction. This can be given as

$$q_i = x_i^1 \xi_1 + x_i^2 \xi_2 + x_i^3 \xi_3 \tag{9}$$

where $i = 1, \ldots, N$ and ξ_k are *modal amplitudes* (i.e. scalars). Substituting equation (9) into the W expression, equation (3), after some manipulation, and keeping only up to fourth order terms, we get

$$W = \frac{1}{2!}(\hat{V}_{ij} + \Lambda \hat{V}_{ijk} Q_k^{\mathrm{F}}) q_i q_j + \frac{1}{3!}(\hat{V}_{ijk} + \Lambda \hat{V}_{ijkl} Q_l^{\mathrm{F}}) q_i q_j q_k + \frac{1}{4!}(\hat{V}_{ijkl}) q_i q_j q_k q_l \tag{10}$$

Hence, the energy W can be written as

$$W = \frac{1}{2!}\delta_{st}\xi_s\xi_t(\Lambda - \Lambda^s) + \frac{1}{3!}(\hat{V}_{ijk} + \Lambda \hat{V}_{ijkl} Q_l^{\mathrm{F}}) x_i^s x_j^t x_k^u \xi_s \xi_t \xi_u + \frac{1}{4!}(\hat{V}_{ijkl}) x_i^s x_j^t x_k^u x_l^v \xi_s \xi_t \xi_u \xi_v \tag{11}$$

becoming a function of ξ_s, $\mathbf{x}_i^s$, and $s, t, u, v = 1, 2, 3$. The complete equilibrium path could be traced if we calculate the mode amplitudes ξ_s. In other words, we have constructed a basis of vectors (the three modes $\mathbf{x}_j^s$) to express the admissible configuration of the system and particularly the equilibrium path, and we now seek to find how these amplitudes change with the evolving path.

At this stage, there are still three unknowns: the values of ξ_s. At an equilibrium state, W must be stationary with respect to all possible variations of the generalized co-ordinates q_i, but the variations are written in terms of the ξ_s. Thus,

$$\frac{\partial W[\xi_t, \Lambda]}{\partial \xi_s} = W_{,s} = 0 \tag{12}$$

for $s = 1, 2, 3$ or else, from equation (11)

$$W_{,s} = 0 = [(\Lambda - \Lambda^s)\delta_{st}]\xi_t + [\tfrac{1}{2}(\hat{V}_{ijk} Q_l^{\mathrm{F}}) x_i^s x_j^t x_k^u]\xi_t\xi_u + [\tfrac{1}{6}(\hat{V}_{ijkl}) x_i^s x_j^t x_k^u x_l^v]\xi_t\xi_u\xi_v \tag{13}$$

Expanding equation (13), we now get three cubic non-linear equations

$$\begin{aligned}
(\Lambda - \Lambda_c^1)\xi_1 &+ A^{111}\xi_1^2 + 2A^{112}\xi_1\xi_2 + A^{122}\xi_2^2 + 2A^{113}\xi_1\xi_3 + 2A^{123}\xi_2\xi_3 + A^{133}\xi_3^2 \\
&+ B^{1111}\xi_1^3 + 3B^{1122}\xi_1\xi_2^2 + 3B^{1112}\xi_1^2\xi_2 + B^{1222}\xi_2^3 \\
&+ B^{1333}\xi_3^3 + 3B^{1133}\xi_1\xi_3^2 + 3B^{1113}\xi_1^2\xi_3 \\
&+ 3B^{1223}\xi_2^2\xi_3 + 3B^{1233}\xi_2\xi_3^2 + 6B^{1123}\xi_1\xi_2\xi_3 = 0
\end{aligned} \tag{14}$$

$$\begin{aligned}
(\Lambda - \Lambda_c^2)\xi_2 &+ A^{211}\xi_1^2 + 2A^{212}\xi_1\xi_2 + A^{222}\xi_2^2 + 2A^{213}\xi_1\xi_3 + 2A^{223}\xi_2\xi_3 + A^{233}\xi_3^2 \\
&+ B^{2111}\xi_1^3 + 3B^{2122}\xi_1\xi_2^2 + 3B^{2112}\xi_1^2\xi_2 + B^{2222}\xi_2^3 \\
&+ B^{2333}\xi_3^3 + 3B^{2133}\xi_1\xi_3^2 + 3B^{2133}\xi_1^2\xi_3 \\
&+ 3B^{2223}\xi_2^2\xi_3 + 3B^{2233}\xi_2\xi_3^2 + 6B^{2123}\xi_1\xi_2\xi_3 = 0
\end{aligned} \tag{15}$$

$$\begin{aligned}
(\Lambda - \Lambda_c^3)\xi_3 &+ A^{311}\xi_1^2 + 2A^{312}\xi_1\xi_2 + A^{322}\xi_2^2 + 2A^{313}\xi_1\xi_3 + 2A^{323}\xi_2\xi_3 + A^{333}\xi_3^2 \\
&+ B^{3111}\xi_1^3 + 3B^{3122}\xi_1\xi_2^2 + 3B^{3112}\xi_1^2\xi_2 + B^{3222}\xi_2^3 \\
&+ B^{3333}\xi_3^3 + 3B^{3133}\xi_1\xi_3^2 + 3B^{3133}\xi_1^2\xi_3 \\
&+ 3B^{3223}\xi_2^2\xi_3 + 3B^{3233}\xi_2\xi_3^2 + 6B^{3123}\xi_1\xi_2\xi_3 = 0
\end{aligned} \tag{16}$$

where

$$A^{stu} = \tfrac{1}{2}(\hat{V}_{ijk} + \Lambda \hat{V}_{ijkl} Q_l^{\mathrm{F}}) x_i^s x_j^t x_k^u$$
$$B^{stuv} = \tfrac{1}{6}\hat{V}_{ijkl} x_i^s x_j^t x_k^u x_l^v \tag{17}$$

Thus, we now have three cubic equations (14)–(16) in three unknowns (ξ_1, ξ_2 and ξ_3), that along with the load Λ describe a four dimensional equilibrium path. By designating the three interacting modes as global, primary local, and secondary local, one can use only the global and primary local mode to graphically represent the post buckling paths of the system.

In the present work, the loads are assumed to be conservative. The potential of the external loads is linear in Q_i and plays a role only in the determination of the fundamental path (equation (2)). All the interacting modes occur in the post-critical state. Since the critical state is assumed to be a bifurcation point, all the modes are orthogonal to the load vector.

3. SHEAR DEFORMABLE FINITE ELEMENT

Following a first-order shear deformation theory, the displacement field is

$$\begin{aligned} u(x, y, z) &= u_0(x, y) - z\theta_x \\ v(x, y, z) &= v_0(x, y) - z\theta_y \\ w(x, y, z) &= w_0(x, y) \end{aligned} \tag{18}$$

where θ_x and θ_y are the average rotations of a line initially perpendicular to the middle surface of the plate (Figure 1). Within each element these displacements can be expressed with respect to nodal unknowns with the aid of the shape functions N_i as

$$(u, v, w, \theta_x, \theta_y, \theta_z) = \sum_{i=1}^{N} N_i(u_i, v_i, w_i, \theta_{x_i}, \theta_{y_i}, \theta_{z_i}) \tag{19}$$

where N is the number of nodes in the finite element. A nine node Lagrangean element has been adopted in this work. For each node, it is convenient to write the vector of unknowns as

$$\{q_i\} = \{u_i \;\; v_i \;\; w_i \;\; \theta_{x_i} \;\; \theta_{y_i} \;\; \theta_{z_i}\}^{\mathrm{T}} \tag{20}$$

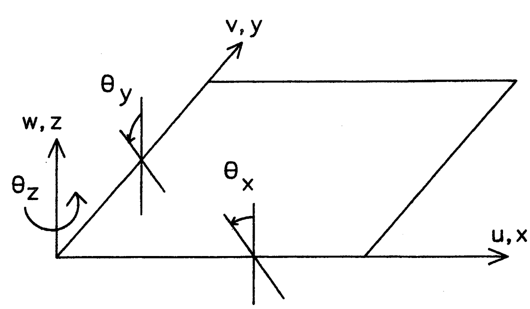

Figure 1. Finite element notation

The strains are written as the summation of a linear plus a non-linear part, leading to

$$\{\varepsilon\} = \{\varepsilon_0\} + \{\varepsilon_1\} = \left\{\begin{matrix} u_{,x} \\ v_{,y} \\ u_{,y} + v_{,x} \\ -\theta_{x,x} \\ -\theta_{y,y} \\ -\theta_{x,y} - \theta_{y,x} \\ -w_{,y} - \theta_y \\ w_{,x} - \theta_x \\ \theta_z \end{matrix}\right\} + \frac{1}{2}\left\{\begin{matrix} v_{,x}^2 + w_{,x}^2 \\ u_{,y}^2 + w_{,y}^2 \\ 2w_{,x}w_{,y} \\ 0 \\ 0 \\ 0 \\ 0 \\ 0 \\ 0 \end{matrix}\right\} \tag{21}$$

where

$$\{\varepsilon\} = \{\varepsilon_x \; \varepsilon_y \; \gamma_{xy} \; \kappa_x \; \kappa_y \; \kappa_{xy} \; \gamma_{yz} \; \gamma_{zx} \; \theta_z\}^{\mathrm{T}} \tag{22}$$

and ε_x, ε_y, and γ_{xy} are the in-plane strains, κ_x, κ_y and κ_{xy} are the curvatures, γ_{yz} and γ_{zx} are the out-of-plane shear strains and θ_z is the in-plane rotation. Note that equation (21) contains not simply the von-Karman equations, but also the terms $\partial v/\partial x$ and $\partial u/\partial y$ are included as in the work of Benito and Sridharan.[22,23] These additional terms are necessary to represent correctly the non-linearities at the junction of flange and web of prismatic columns, mainly for the modal interaction analysis.

Using FE notation,[39] the matrix $[B_0]$ results from the Mindlin–Reissner assumptions.[40] The matrix $[B_1]$ is a function of the nodal displacements, i.e. $[B_1(q)]$. Following Zienkiewicz and Taylor[39] we can write the non-linear part of the strains as

$$\{\varepsilon_1\} = \tfrac{1}{2}[A][\theta] = [B_1(q)]\{q\} \tag{23}$$

where the matrices $[A]$ and $[\theta]$ are still a function of the nodal displacements. The matrix $[\theta]$ can be written as $[\theta] = [G]\{q\}$ with the matrix $[G]$ constructed in a similar way to Zienkiewicz and Taylor (Reference 39 Section 8.3, Vol. 2). Taking the variation of equation (23) it is possible to write $d\{\varepsilon_1\} = [A][G]d\{q\}$. Therefore, it follows that $[2B_1] = [A][G]$. On the other hand, the matrix $[A(q)]$ can be written as the product of two matrices, the first containing the derivatives of the shape functions and the second the nodal displacements, as

$$[A(q)] = \begin{bmatrix} 0 & N_{i,x} & N_{i,x} & 0 \\ N_{i,y} & 0 & 0 & N_{i,y} \\ 0 & 0 & N_{i,y} & N_{i,x} \\ 0 & 0 & 0 & 0 \\ 0 & 0 & 0 & 0 \\ 0 & 0 & 0 & 0 \\ 0 & 0 & 0 & 0 \\ 0 & 0 & 0 & 0 \\ 0 & 0 & 0 & 0 \end{bmatrix} \begin{bmatrix} \{q\} & 0 & 0 & 0 \\ 0 & \{q\} & 0 & 0 \\ 0 & 0 & \{q\} & 0 \\ 0 & 0 & 0 & \{q\} \end{bmatrix} \tag{24}$$

The total potential energy W of the plate subjected to in-plane and transverse loading can now be written as

$$W = \frac{1}{2}\int \{\sigma\}^{\mathrm{T}}\{\varepsilon\}\,\mathrm{d}v - \Lambda\{q\}^{\mathrm{T}}\{f\} \tag{25}$$

The load vector $\{f\}$ is assumed to be incremented by a single load factor Λ. The stress vector $\{\sigma\}$ is in this case

$$\{\sigma\} = \{N_x\ N_y\ N_{xy}\ M_x\ M_y\ M_{xy}\ Q_y\ Q_x\ M_z\}^{\mathrm{T}} \tag{26}$$

where N_x, N_y and N_{xy} are the in-plane stress resultants, M_x, M_y and M_{xy} are the moment resultants, Q_y and Q_x are the out-of-plane shear stress resultants and M_z is the in-plane moment. For the case of a plate made of laminated composite material, the constitutive law is

$$\begin{Bmatrix} N_x \\ N_y \\ N_{xy} \\ M_x \\ M_y \\ M_{xy} \\ Q_y \\ Q_x \\ M_z \end{Bmatrix} = \begin{bmatrix} A_{11} & A_{12} & A_{16} & B_{11} & B_{12} & B_{16} & 0 & 0 & 0 \\ A_{12} & A_{22} & A_{26} & B_{12} & B_{22} & B_{26} & 0 & 0 & 0 \\ A_{16} & A_{26} & A_{66} & B_{16} & B_{26} & B_{66} & 0 & 0 & 0 \\ B_{11} & B_{12} & B_{16} & D_{11} & D_{12} & D_{16} & 0 & 0 & 0 \\ B_{12} & B_{22} & B_{26} & D_{12} & D_{22} & D_{26} & 0 & 0 & 0 \\ B_{16} & B_{26} & B_{66} & D_{16} & D_{26} & D_{66} & 0 & 0 & 0 \\ 0 & 0 & 0 & 0 & 0 & 0 & A_{44} & A_{45} & 0 \\ 0 & 0 & 0 & 0 & 0 & 0 & A_{45} & A_{55} & 0 \\ 0 & 0 & 0 & 0 & 0 & 0 & 0 & 0 & C^* \end{bmatrix} \begin{Bmatrix} \varepsilon_x \\ \varepsilon_y \\ \gamma_{xy} \\ \kappa_x \\ \kappa_y \\ \kappa_{xy} \\ \gamma_{yz} \\ \gamma_{zx} \\ \theta_z \end{Bmatrix} \tag{27}$$

where, A_{ij}, B_{ij} and D_{ij} are the plate stiffness properties as computed using the Classical Lamination Theory[41,42] and C^* is a very small number compared to the stiffness values, that corresponds to in-plane rotation θ_z.[43]

Materials with non-vanishing bending-extension coupling terms B_{ij} are modelled here with an approximate linear fundamental path. The limitations of this approach are being investigated.[44]

4. STABILITY OF THE DISCRETIZED SYSTEM

As a first step, the linear fundamental path $\{Q^{\mathrm{F}}\}$ should be obtained. The stiffness matrix $[K_0]$ is needed, and can be formulated following Zienkiewicz and Taylor.[39] Solving the equilibrium equations with respect to $\{Q^{\mathrm{F}}\}$, we determine the pre-buckling solution. The second step is the detection of the critical states along the fundamental path. For this reason, it is necessary to compute the geometric stiffness matrix $[K_\sigma]$. This can be done following Zienkiewicz and Taylor (1991). The critical states, i.e. the critical loads Λ^{C} and the corresponding eigenvectors $\{x\}$, are determined solving the classical eigenvalue problem.

Next, attention is given to the study of the post critical path passing through the bifurcation point. First, we must determine whether the bifurcation is symmetric or asymmetric. For that, it is necessary to compute the matrix $[D_1(x)]$ contracted by the eigenvector $\{x\}$. This can be written in terms of finite element matrices as

$$[D_1(x)] = \int_V \{[2B_1^i(\delta_j)]^T [C] [B_0 + 2\Lambda B_1(Q^F)] \{x\} + [2B_1(x)]^T [C] [B_0 + 2\Lambda B_1(Q^F)] + [B_0 + 2\Lambda B_1(Q^F)]^T [C] [2B_1(x)]\} \, dv \tag{28}$$

where δ_i is the Kroneker delta, with values $\delta_i = 1$, if $i = j$, and $\delta_i = 0$, if $i \neq j$. The matrix $[2B_1^i(\delta_j)]$ can be computed from $[2B_1] = [A][G]$ if in the second matrix of equation (24) instead of $\{q\}$, we insert a vector containing unit value in the jth row and zeros in the rest.

The coefficient C may now be computed as

$$C = \{x\}^T [D_1(x)] \{x\} \tag{29}$$

If $C = 0$, the critical state is a symmetric bifurcation; while for $C \neq 0$ the bifurcation is asymmetric. To follow the post buckling path, a perturbation analysis is carried out from the critical state. The variables q_i and Λ are expanded in terms of a perturbation parameter q_1, as indicated in equation (5). For symmetric bifurcation, the slope $\Lambda^{(1)C}$ of the post-buckling path at the bifurcation point vanishes, and $\{q^{(1)C}\} \equiv \{x\}$. As a next step, the $\{q^{(2)C}\}$ coefficients in equation (5) are computed from

$$[K_T] \{q^{(2)C}\} = -[D_1(x)] \{x\}|^C \tag{30}$$

where $[K_T] = [K_0] + \Lambda [K_\sigma]$ is the tangential stiffness matrix at the critical state. The value of one of the components in the vector of the second derivatives of the displacements has to be chosen (i.e. $q_1^{(2)C} = 0$ if the perturbation parameter is q_1). Finally, the curvature of the post-buckling path at the bifurcation point results in

$$\Lambda^{(2)C} = -\frac{\{x\}^T [D_2(x,x)] \{x\} + 3\{x\}^T [D_1(x)] \{q^{(2)C}\}}{3\{x\}^T [K_\sigma] \{x\}} \tag{31}$$

The matrix $[D_2(x, x)]$ contracted by the $\{x\}$ eigenvector can be computed from

$$[D_2(x,x)] = \int_V \{[2B_1^i(\delta_j)]^T [C] [2B_1(x)] \{x\} + 2[2B_1(x)]^T [C] [2B_1(x)]\} \, dv \tag{32}$$

The coefficients A^{stu} (equation (17)) of the quadratic terms in the equilibrium equations are related to the contracted matrix $[D_1(\mathbf{x})]$ in the following manner:

$$A^{stu} = \tfrac{1}{2} x_i^s [D_1(x_j^t)] x_k^u \tag{33}$$

But since the contracted matrix $[D_1(\mathbf{x})]$ is a function of the load parameter Λ (equation (28)), we can write

$$A^{stu} = \tfrac{1}{2} x_i^s \{[E_1(x_j^t)] + \Lambda [E_2(x_j^t)]\} x_k^u \tag{34}$$

where

$$\begin{aligned} [E_1(x)] &= \int \{[2B_1(\delta)]^T [C] [B_0] \{x\} + [2B_1(x)]^T [C] [B_0] + [B_0]^T [C] [2B_1(x)]\} \, dv \\ [E_2(x)] &= \int \{[2B_1(\delta)]^T [C] [2B_1(q^F)] \{x\} + [2B_1(x)]^T [C] [2B_1(q^F)] \\ &\quad + [2B_1(q^F)]^T [C] [2B_1(x)]\} \, dv \end{aligned} \tag{35}$$

or

$$A^{stu} = F^{stu} + \Lambda G^{stu} \tag{36}$$

where

$$F^{stu} = \tfrac{1}{2} x_i^s E_1(x_j^t) x_k^u$$
$$G^{stu} = \tfrac{1}{2} x_i^s E_2(x_j^t) x_k^u \tag{37}$$

The coefficients B^{stuv} (equation (17)) of the cubic terms in the equilibrium equations are related to the contracted matrix $[D_2(\mathbf{x}, \mathbf{y})]$ in the following manner:

$$B^{stuv} = \tfrac{1}{6} x_i^s [D_2(x_j^t, x_k^u)] x_l^v \tag{38}$$

Note that the energy terms are symmetric in the sense that

$$A^{stu} = A^{tus} = A^{ust}$$
$$B^{stuv} = B^{tuvs} = B^{uvst} = B^{vstu} \tag{39}$$

and hence the necessary computations can be reduced. Finally, the three equilibrium equations (14)–(16) reduce to three non-linear equations

$$(\Lambda - \Lambda^s)\delta_{st}\xi_t + A^{stu}\xi_t\xi_u + B^{stuv}\xi_t\xi_u\xi_v = 0 \tag{40}$$

where $s, t, u, v = 1, 2, 3$. These equations are then solved by numerical or perturbation techniques.

The imperfection sensitivity of the system can be investigated by using the imperfection parameters $\bar{\xi}_i$, if it is assumed that the system has an imperfection of the same shape as the corresponding eigenmode, the amplitude of which is $\bar{\xi}_i$. The equilibrium equations for the imperfect case of three interacting modes become

$$(\Lambda - \Lambda^s)\delta_{st}\xi_t + A^{stu}\xi_t\xi_u + B^{stuv}\xi_t\xi_u\xi_v = \Lambda\bar{\xi}_t \tag{41}$$

where $s, t, u, v = 1, 2, 3$. Usually, the imperfection sensitivity is studied for various values of $\bar{\xi}_1$ and $\bar{\xi}_2$, that correspond to the global and primary local mode, while $\bar{\xi}_3$ (that corresponds to the secondary local mode) is set to zero. Equation (41) can be solved using numerical techniques such as Newton–Raphson.

5. NUMERICAL RESULTS

To illustrate the numerical procedure, we consider a composite I-column. The geometry of the column is defined by $b = 6$ in; $h = 6$ in, and $L = 100$ in. The material properties for the flanges with reference to equation (27) are: $A_{11} = 893\,500$ lb/in; $A_{22} = 343\,000$ lb/in; $A_{12} = 130\,800$ lb/in; $A_{66} = 113\,600$ lb/in; $D_{11} = 4289$ lb in; $D_{22} = 2029$ lb in; $D_{12} = 807{\cdot}3$ lb in; $D_{66} = 641{\cdot}5$ lb in, $A_{44} = A_{55} = 94\,670$ lb/in; and $A_{45} = A_{54} = 0$. For the web the material properties are $A_{11} = 893\,500$ lb/in; $A_{22} = 343\,000$ lb/in; $A_{12} = 130\,800$ lb/in; $A_{66} = 113\,600$ lb/in; $D_{11} = 4090$ lb in; $D_{22} = 1863$ lb in; $D_{12} = 731{\cdot}6$ lb in; $D_{66} = 596{\cdot}1$ lb in, $A_{44} = A_{55} = 94670$ lb/in; and $A_{45} = A_{54} = 0$. The column is discretized to 45 elements as shown in the mesh in Figure 2. The boundary conditions applied to the FE model are simply supported ends where the rotation about the weak axis of the cross section is free. Hence, a global mode (Euler) is expected to occur about the weak axis.

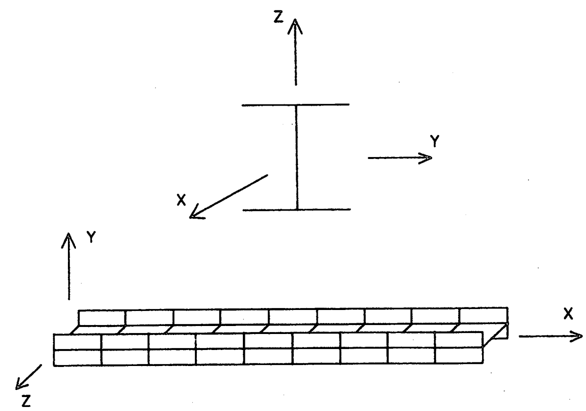

Figure 2. Finite element mesh for the I-column

5.1. *Perfect system*

The model is first solved for pre-buckling displacements, and the eigenvalue problem is then formulated. As a result, the critical buckling loads and the associated eigenmodes are determined. A selected number of critical loads that are the eigenvalues of the buckling problem are shown in Table I. A mode number is assigned to each eigenvalue with reference to Figure 3. Figure 3 contains schematics of the modal shapes associated with the eigenvalues presented in Table I. Each mode is represented by the cross-sectional modal deformation at the $x = L/2$, the lateral deformation of the longitudinal axis passing through the centroid for the entire length of the column, and the lateral deformation of the right tip of the top flange for the entire length as well.

The lowest eigenvalue (Mode # 1242 in Table I) corresponds to the primary local buckling mode, and is $\Lambda^1 = 27\,323$ lb. The associated eigenmode $\mathbf{x}^1$ can be seen in Figures 3 and 4. Both the flanges rotate and the web bends with eight waves along the length of the column. An isolated mode post-buckling analysis shows that the secondary equilibrium path for the primary local mode is stable symmetric (Figure 5) and the curvature is found to be* $\Lambda_1^{(2)C} = -172\,182$ lb/in^2.

The global mode $\mathbf{x}^2$ (Euler about weak axis) is next identified from Figure 3 (Mode # 1246). The cross-section remains undeformed but the whole beam buckles with one wave in the global sense. The critical load is $\Lambda^2 = -29\,761$ lb (Table I). The post-buckling path has found to be also stable symmetric and the curvature is computed as $\Lambda_2^{(2)C} = -211$ lb/in^2, that is a low value, compared to the one of the local post buckling path.

The secondary local mode, that combined with the other two will produce interaction and will change the stable post buckling behaviour of the I-beam into an unstable path, is next selected. The third mode will have a flange waviness, with no web distortion. From Figure 3, we see that there is a mode that may be suitable to interact with the two modes already selected. The chosen one (Mode # 1241) corresponds to a critical load $\Lambda^3 = -142\,923$ lb, that is very close to the

*A subscript indicates a mode number

Table I. Critical modes and corresponding critical loads for the pultruded I-column

Mode	Critical Load
1231	– 193 994·50
1232	– 191 354·23
1233	– 189 244·32
1234	– 171 387·39
1235	– 175 405·49
1236	– 174 636·60
1237	– 196 773·89
1238	– 198 689·01
1239	– 179 645·15
1240	– 160 458·93
1241	– 142 923·56
1242	– 27 323·60
1243	– 27 461·80
1244	– 29 048·20
1245	– 29 432·43
1246	– 29 761·56
1247	– 31 698·91
1248	– 33 527·09
1249	– 142 770·19
1250	– 36 572·63
1251	– 129 134·71
1252	– 122 922·03
1253	– 40 905·58
1254	– 36 342·64
1255	– 44 589·87
1256	– 55 340·84
1257	– 38 960·76
1258	– 60 111·63
1259	– 40 119·62
1260	– 42 739·29
1261	– 43 760·90
1262	– 47 486·69
1263	– 117 812·37
1264	– 131 584·77
1265	– 115 168·30
1266	– 128 594·97

value of the third load in the simplified model analysis of Godoy *et al.*[45] The post critical path is also stable symmetric.

Next, the eigenvectors of the three selected modes are normalized according to equation (8), where the highest components are: 4.48 for the global mode $\mathbf{x}^1$, 1·6755 for the primary local mode $\mathbf{x}^2$, and 1·369 for the secondary local mode $\mathbf{x}^3$. The coefficients F^{stu}, G^{stu} and B^{stuv} in equations (37)–(38) (where $s, t, u, v = 1, 2, 3$) of the three equilibrium equations (40) in modal space, are then computed. The numerical values of the interaction coefficients that are different from zero are: $F^{113} = -395{\cdot}6$, $F^{123} = -5628{\cdot}4$, $F^{223} = -1590{\cdot}2$, $F^{333} = -708{\cdot}2$, $G^{113} = -1{\cdot}558 \times 10^{-3}$, $G^{123} = 5{\cdot}931 \times 10^{-4}$, $G^{223} = -1{\cdot}768 \times 10^{-3}$, $G^{333} = -0{\cdot}15673$, $B^{1111} = 2\,701\,272$, $B^{1112} = -2\,500$, $B^{1122} = 64\,993$, $B^{1133} = 1\,839\,560$, $B^{1222} = -210{\cdot}6$, $B^{1233} = 7\,681$, $B^{2222} = 174\,216$, $B^{2233} = 230\,266$ and $B^{3333} = 15\,007\,517$. Hence, the following equilibrium equations are defined

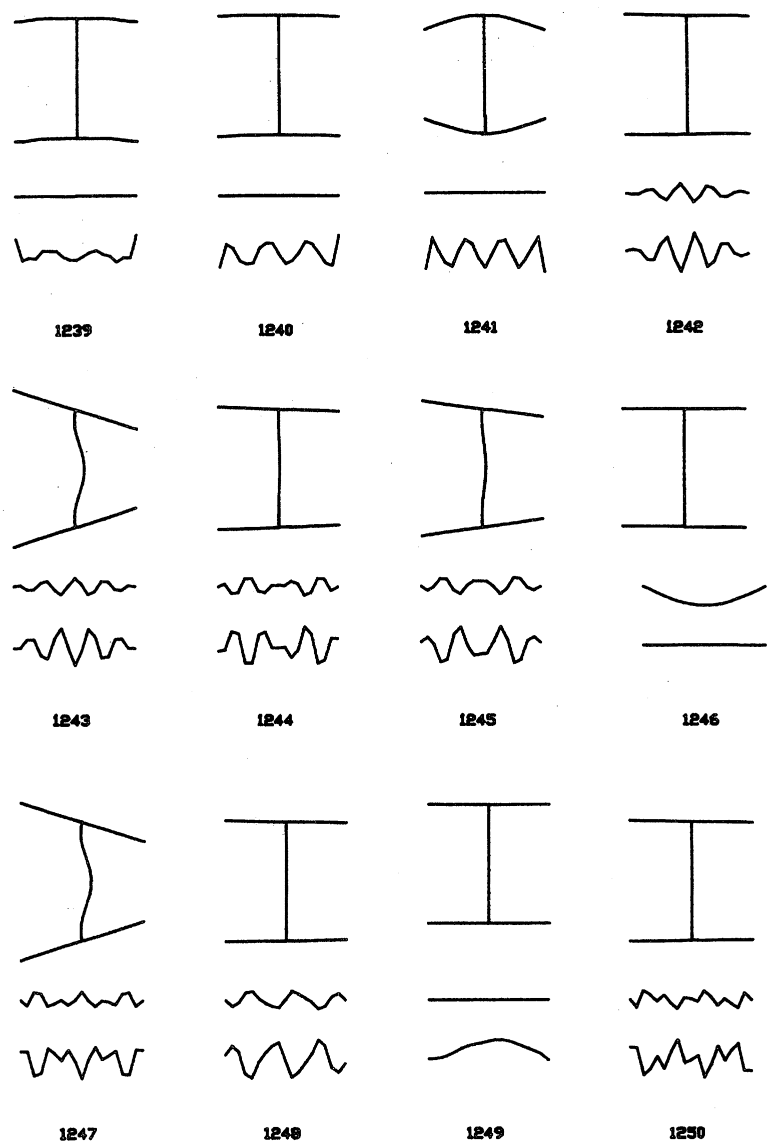

Figure 3. Modal shapes for the I-column

and can be solved for specified values of the load parameter Λ:

$$\begin{aligned}
&(\Lambda + 27\,323)\xi_1 - (791{\cdot}2 + 0{\cdot}003116\Lambda)\xi_1\xi_3 - (11256{\cdot}8 - 0{\cdot}0011862\Lambda)\xi_2\xi_3 + 270\,1272\xi_1^3 \\
&\quad - 7500\xi_1^2\xi_2 + 194\,979\xi_1\xi_2^2 + 5\,518\,680\xi_1\xi_3^2 + 23\,043\xi_2\xi_3^2 - 210{\cdot}6\xi_2^3 = 0 \\
&(\Lambda + 29\,761)\xi_2 - (11256{\cdot}8 - 0{\cdot}0011862\Lambda)\xi_1\xi_3 - (3180{\cdot}4 + 0{\cdot}003536\Lambda)\xi_2\xi_3 - 2500\xi_1^3 \\
&\quad + 194\,979\xi_1^2\xi_2 + 690\,798\xi_2\xi_3^2 - 631{\cdot}8\xi_1\xi_2^2 + 17\,421\xi_2^3 + 23\,043\xi_1\xi_3^2 = 0 \\
&(\Lambda + 142\,923)\xi_3 - (395{\cdot}6 + 0{\cdot}001558\Lambda)\xi_1^2 - (11256{\cdot}8 - 0{\cdot}0011862\Lambda)\xi_1\xi_2 \\
&\quad - (1590{\cdot}2 + 0{\cdot}001768\Lambda)\xi_2^2 - (708{\cdot}2 + 0{\cdot}15673\Lambda)\xi_3^2 + 150\,07517\xi_3^3 \\
&\quad + 5\,518\,680\xi_1^2\xi_3 + 690\,798\xi_2^2\xi_3 + 46\,086\xi_1\xi_2\xi_3 = 0
\end{aligned} \tag{42}$$

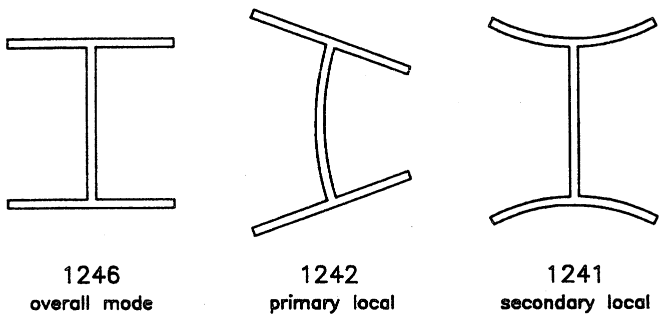

Figure 4. Schematics of the three interacting modes

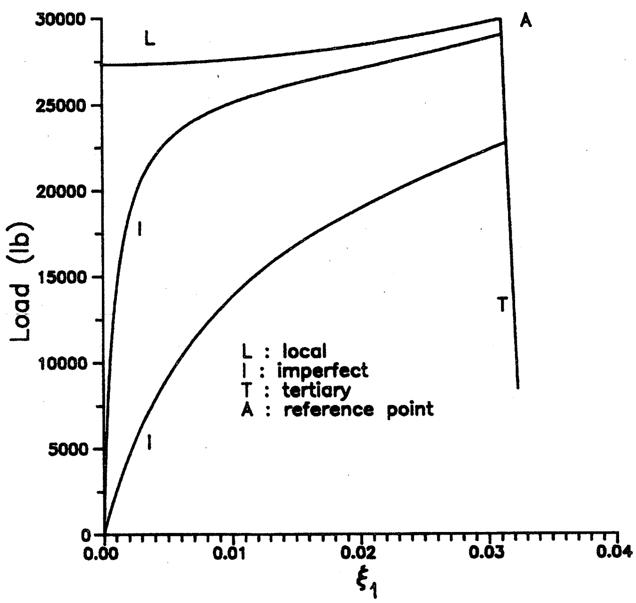

Figure 5. Equilibrium path projection on Λ–ξ_1 plane (local)

Notice that by keeping the coefficients B^{1111}, B^{2222} and B^{3333}, while setting all the rest equal to zero, we retrieve the equilibrium equations corresponding to the secondary post buckling path for the isolated mode case. In order to study possible interaction between the modes, we see that the coefficients which couple all three modes are of significant importance.

Next, in order to determine the tertiary (coupled) path, we expect the system to experience loss of stability. According to the mode interaction theory, the tertiary path will be branching from the lower secondary path, which corresponds to the primary local mode. Hence, selecting ξ_1 as perturbation parameter we can write

$$\begin{aligned}\Lambda &= \Lambda^{(0)} + \Lambda^{(1)}\xi_1 + \tfrac{1}{2}\Lambda^{(2)}\xi_1^2 \\ \xi_2 &= \xi_2^{(0)} + \xi_2^{(1)}\xi_1 + \tfrac{1}{2}\xi_2^{(2)}\xi_1^2 \\ \xi_3 &= \xi_3^{(0)} + \xi_3^{(1)}\xi_1 + \tfrac{1}{2}\xi_3^{(2)}\xi_1^2\end{aligned} \tag{43}$$

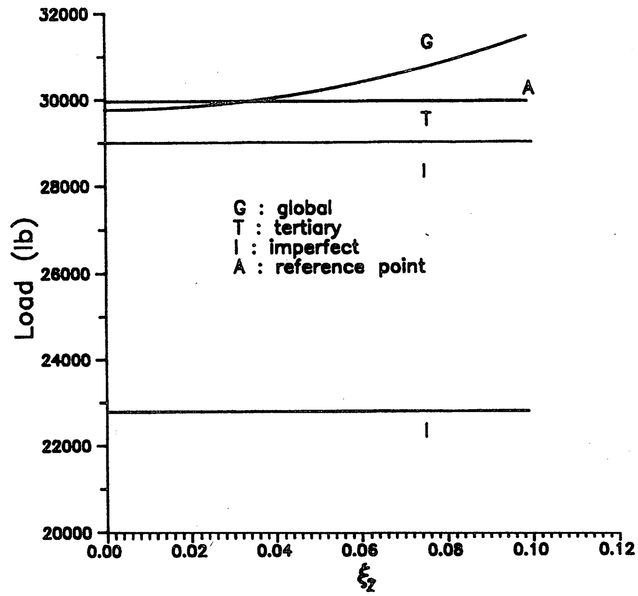

Figure 6. Equilibrium path projection on Λ–ξ_2 plane (global)

Since we are following the secondary path, we can directly set $\xi_2^{(0)} = 0$ and $\xi_3^{(0)} = 0$. The bifurcation on the secondary path is then computed by simultaneously solving the isolated path equilibrium equation, that is

$$\Lambda + 27\,323 + 2\,701\,272\xi_1^2 = 0 \tag{44}$$

and the stability determinant equation $|W_{ij}| = 0$ $(i, j = 1, 2, 3)$, in terms of the reduced energy W (equation (11)). Hence, we get $\Lambda^{(0)} = -29\,950{\cdot}1$ and $\xi_1^{(0)} = 0{\cdot}031182$. The first-order perturbation coefficients are given by $\Lambda^{(1)} = -7255$; $\xi_2^{(1)} = 683{\cdot}3$ and $\xi_3^{(1)} = 2{\cdot}03$, and the second-order coefficients are $\Lambda^{(2)} = 3{\cdot}57 \times 10^{11}$; $\xi_2^{(2)} = 2{\cdot}28 \times 10^9$ and $\xi_3^{(2)} = 2{\cdot}03 \times 10^6$.

Since, $\Lambda < 0$ and all $\xi_i > 0$, we see that on the tertiary path Λ–ξ_1, the load-carrying capacity decreases (loss of stability) for increasing ξ_1. The secondary local and global paths, the bifurcation on the secondary local, and the emerging tertiary paths are shown in Figure 5 (projection on the Λ–ξ_1 plane, ξ_1 being the amplitude of the local mode) and in Figure 6 (projection in the Λ–ξ_2 plane, ξ_2 being the amplitude of the global mode).

The non-linear path resulting from the analysis of the imperfect system is also shown. The tertiary path in Λ–ξ_1 plane seems to fall abruptly. However, the path really is contained in the Λ–ξ_2 plane with shallow slope indicative of mild imperfection sensitivity. Point A was labeled on both path to aid in the interpretation of Figure 6.

For comparison, we can use the results of a simplified model[45] based on a three-parameter Ritz discretization of the problem. The critical loads that correspond to primary local mode (bending of the web and rotation of the flanges), global buckling (Euler) about the weak axis, and secondary local mode (bending of the flanges only) are $\Lambda_1^C = -30\,021{\cdot}9$ lbs, $\Lambda_2^C = -28\,633{\cdot}7$ lb, and $\Lambda_3^C = -142\,422{\cdot}6$ lb. The three interacting eigenmodes have been normalized, and the highest components are: 4·5 for the global mode $\mathbf{x}^1$, 0·968 for the primary local mode $\mathbf{x}^2$, and 1·369 for the secondary local mode $\mathbf{x}^3$. The difference in the local mode normalization component is due to the amplitude modulation (observed in the FE analysis but lacking in the simplified

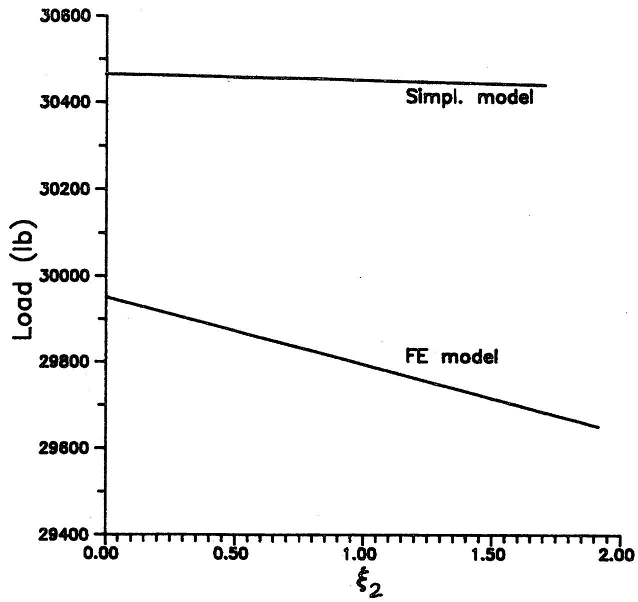

Figure 7. Comparison between simple and FE model (equilibrium path projection on Λ–ξ_2, global)

model) and to slight bending of the flanges in the FE analysis, that the simplified model cannot account for.

Using the energy terms computed in the simplified model analysis, we recalculate equation (42). The numerical values of the non-zero coefficients are: $F^{113} = 21$, $F^{123} = 45\,409{\cdot}8$, $G^{113} = -5{\cdot}981 \times 10^{-3}$; $B^{1111} = 328\,740{\cdot}8$, $B^{1122} = 45\,218{\cdot}3$, $B^{1133} = 2\,096\,787{\cdot}9$, $B^{2222} = 175\,092$, $B^{2233} = 162\,416{\cdot}2$, and $B^{3333} = 12\,196\,023$. Hence, the equilibrium equations (40) can be solved using the perturbation scheme (43). As a result, we get $\Lambda^{(0)} = -30\,464{\cdot}9$ and $\xi_1^{(0)} = 0{\cdot}074635$. The first-order perturbation coefficients are given by $\Lambda^{(1)} = -48\,735$, $\xi_2^{(1)} = 17{\cdot}01$ and $\xi_3^{(1)} = -0{\cdot}7849$, and the second-order coefficients are $\Lambda^{(2)} = 2{\cdot}03 \times 10^8$; $\xi_2^{(2)} = 1{\cdot}37 \times 10^7$ and $\xi^{(2)} = 6{\cdot}33 \times 10^5$. We see that the bifurcation load $\Lambda^{(0)}$, as well as the amplitude $\xi_1^{(0)}$, have different values than the ones in FE model. Also, the perturbation coefficients of the simplified model are of smaller magnitude than the ones of the FE model. The differences are due to the different normalization components. The FE and the simplified model agree in that the load on the tertiary path Λ–ξ_1 decreases for increasing ξ_1. The projection of the tertiary path Λ–ξ_2 is plotted in Figure 7 for the FE model and the simplified model, when keeping the cubic terms. The projection of the tertiary path on the Λ–ξ_3 plane is plotted in Figure 8.

It is worth mentioning that other modes with shape similar to mode 1241 have been chosen as third interacting mode along with 1242 and 1246, and the interaction analysis gives the same bifurcation point ($\Lambda^{(0)}$, $\xi_1^{(0)}$), and similar tertiary path. This means that interaction depends exclusively on the two primary modes. The third mode needs to be considered because first order field is insufficient to trigger interaction.

5.2. Imperfect system

We now consider the I-column having in the unloaded state an initial imperfection similar to the one of the buckled mode shapes, global or local. The amplitude is defined by the imperfection

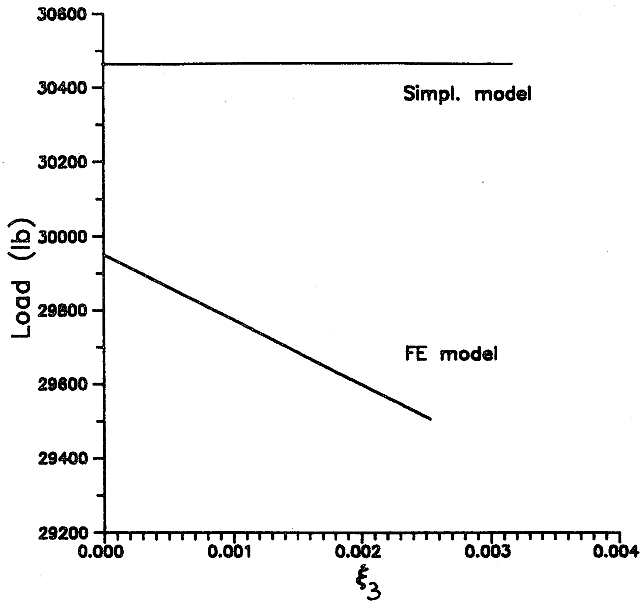

Figure 8. Comparison between simple and FE model (equilibrium path projection on Λ–ξ_3, secondary local)

parameter $\bar{\xi}_i$. Then, the equilibrium equations (41) hold for the imperfect system and are expressed in the modal space. Introduction of the imperfection parameters into equation (41) destroys the primary bifurcation (intersection of primary equilibrium path and secondary path corresponding to the primary local mode). The primary equilibrium path remains stable, but becomes non-trivial. On the other hand, the secondary bifurcation (intersection of the secondary and tertiary path) 'slides' to a new position characterized by larger displacements and lower load. Hence, the load-carrying capacity of the imperfect system is reduced compared to the one of the perfect system.

The three equilibrium equations (41) are solved by the Newton–Raphson technique and the non-linear path is shown in Figures 5 and 6 along with the results of the perfect system analysis. Note that in the Λ–ξ_1 plane (local buckling) the non-linear path seems to stop on the tertiary path. In fact, the non-linear path turns into the Λ–ξ_2 plane that corresponds to global buckling.

The maximum loads on the non-linear imperfect paths for varying value of imperfection are used to construct the imperfection sensitivity curves shown in Figure 9. Here, $\bar{\xi}_1$ is a local mode imperfection, while $\bar{\xi}_2$ is a global mode imperfection. The imperfection sensitivity curves shown in Figure 9 show that the I-column has low imperfection sensitivity, i.e. for a significantly imperfect column, the reduction on the carrying capacity is about 30 per cent. Hence, the system experiences loss of stability when the load reaches a specific value, but small imperfections do not significantly affect this value. For example, one can recall that shells experience significant drop on load carrying capacity for small imperfection amplitudes.

6. CONCLUSIONS

A numerical procedure based on the finite element method and perturbation techniques was developed for post-buckling analysis of structures modelled as plate assemblies. The effect of three

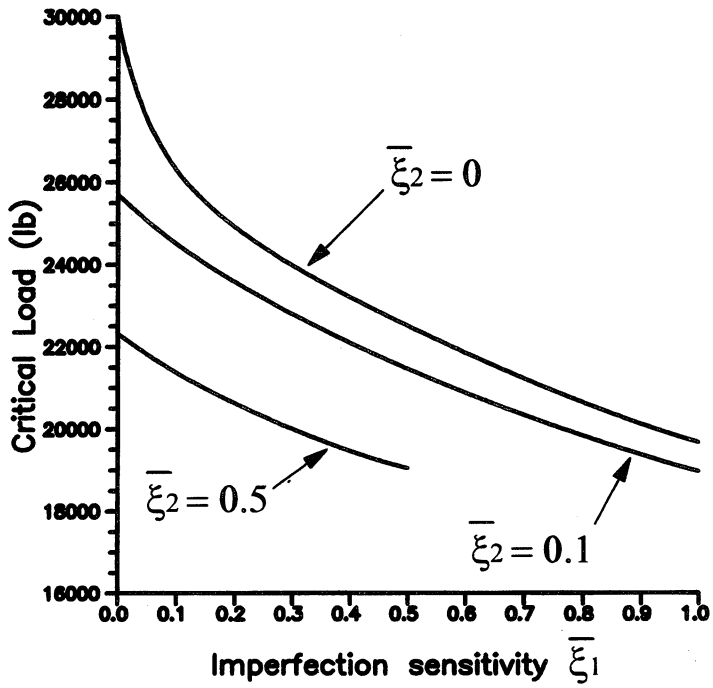

Figure 9. Imperfection sensitivity curves

interacting modes on the post-buckling behaviour was accounted by studying the equilibrium paths in the reduced modal space of active co-ordinates. While the perturbation approach requires computation of fourth-order derivatives of the potential energy, an efficient algorithm was developed by taking advantage of contracted matrices.

A further simplification was obtained by studying the active co-ordinates related to the three interacting modes only. The resulting three non-linear equations describe the complete behaviour of the system in the vicinity of the equilibrium paths. These equations were conveniently solved by perturbation techniques for the perfect paths. For the imperfection analysis, a Newton–Raphson technique was used taking advantage of the knowledge of the perfect primary, secondary, and tertiary paths, the latter arising from mode interaction.

By using a finite element discretization as plate assemblies, all buckling modes (local and global) as well wave amplitude modulation are automatically taken into account. A fibre-reinforced composite column was analysed and the result favourably agree with the results of a simplified model. While all the isolated mode secondary paths were found to be stable, the column was found to be imperfection sensitive once mode interaction was acknowledged.

ACKNOWLEDGEMENTS

This project was partially sponsored by NSF Grant 8802265 and West Virginia Department of Highways Grant RPT699. The financial support is gratefully acknowledged. Luis Godoy was visiting Professor at West Virginia University during the period of this research. Our recognition to Dr. Hota V. S. Ganga Rao, Director, Constructed Facilities Center, for his help and comments about this work.

APPENDIX

Notation

V	total potential energy
$V_0, V_i, V_{ij}, V_{ijk}, V_{ijkl}$	coefficients of V
N	number of degrees of freedom
Q_i	generalized displacements
q_i	incremental generalized displacements
Q_i^F	linear fundamental path for a unit load
W	incremental total potential energy
Λ	load parameter
Λ^C	critical load
$\Lambda^{(1)C}, \Lambda^{(2)C}$	coefficients in the perturbation expansion of the load, slope and curvature, respectively
$q_i^{(1)C}, q_i^{(2)C}$	coefficients in the perturbation expansion of the incremental displacements
$\mathbf{x}^n$	eigenmodes
Λ^n	critical loads
δ_{mn}	Kroneker symbol
ξ_1, ξ_2, ξ_3	amplitude of the interacting modes
u, v, w	continuous displacement field
u_0, v_0, w_0	in-plane displacements
$\theta_x, \theta_y, \theta_z$	rotations of the normal line
$\{\varepsilon\}$	strain vector
$\{\varepsilon_0\}$	linear strain vector
$\{\varepsilon_1\}$	non-linear strain vector
$\varepsilon_x, \varepsilon_y, \gamma_{xy}$	in-plane strains
k_x, k_y, k_{xy}	curvatures
γ_{yz}, γ_{zx}	shear strains
$[B_0]$	linear strain–displacement matrix
$[B_1]$	non-linear strain–displacement matrix
N_i	shape functions
$\{f\}$	load vector
$\{\sigma\}$	stress vector
N_x, N_y, N_{xy}	in-plane stress resultants
M_x, M_y, M_{xy}	moment resultants
Q_x, Q_y	out-of-plane stress resultants
M_z	torsional moment
A_{ij}, B_{ij}, D_{ij}	plate stiffnesses
C^*	rotation stiffness
$[K_\sigma]$	geometric stiffness matrix
C	nature of the critical state
$[D_1], [D_2]$	intermediate calculation matrices
$[K_T]$	tangent stiffness matrix
$\bar{\xi}_i$	amplitude of the imperfection in mode 'i'
$\xi_i^{(0)}, \xi_i^{(1)}, \xi_i^{(2)}$	coefficients of the perturbation expansion of ξ_i
$\Lambda^{(0)}, \Lambda^{(1)}, \Lambda^{(2)}$	coefficients of the perturbation expansion of Λ in the imperfection sensitivity model. $\Lambda^{(0)}$ is the critical load.

REFERENCES

1. J. M. Thompson and G. M. Lewis, 'On optimum design of thin-walled compression members', *J. Mech. Phys. Solids*, **20,** 101–109, (1972).
2. J. M. Thompson and T. M. Lewis, 'Continuum and finite element branching studies of the circular plate', *Comput. Struct.*, **2,** 511 (1972).
3. C. P. Ellinas, *et. al.*, 'Tests on interactive buckling of stiffened plates', *Exp. Mech.*, 455–462 (1977).
4. E. J. Barbero and J. Tomblin, 'A phenomenologic design equation for FRP columns with interaction between local and global buckling', *Thin Walled Struct.*, **18,** 117–131 (1994).
5. A. R. Vakiener, A. Zureick and K. M. Will, 'Prediction of local flange buckling in pultruded shapes by finite element analysis', in S. L. Iyer (ed.), *Adv. Composite Materials in Civil Eng. Structures*, ASCE, New York, 1991, pp. 302–312.
6. Mottran
7. J. M. Thompson and G. W. Hunt, *A General Theory of Elastic Stability*, Wiley, New York, 1973.
8. F. G. Flores, and L. A. Godoy, 'Elastic post buckling analysis via finite element and perturbation techniques. Part 1: Formulation', *Int. j. numer. methods eng.*, **33,** 1775–1794 (1992).
9. A. H. Chilver, 'Coupled modes of elastic buckling', *J. Mech. Phys. Solids*, **15,** 15–28 (1967).
10. A. H. Chilver and K. C. Johns, 'Multiple path generation at coincident branching points, *Int. J. Mech. Sci.*, **13,** 899–910 (1971).
11. J. M. Thompson and W. J. Supple, 'Erosion of optimum designs by compound branching phenomena', *J. Mech. Phys. Solids*, **21,** 135–144 (1973).
12. S. E. Swanson and J. G. A. Croll, 'Interaction between local and overall buckling', *Int. J. Mech. Sci.*, 307–321 (1975).
13. A. C. Walker, 'Interactive buckling of structural components', *Sci. Progress*, **62,** 579–597 (1975).
14. A. J. Reis, 'Interactive buckling in elastic structures', *Ph.D. Thesis*, University of Waterloo, Ont., Canada, 1977.
15. A. J. Reis, and J. Roorda, 'Non linear interactive buckling: sensitivity and optimality', *J. Struct. Mech.*, **5,** 207–232, (1977).
16. A. J. Reis and J. Roorda, 'Post buckling behavior under mode interaction', *J. Eng. Mech.*, **105,** 609–621 (1979).
17. R. Maaskant, 'Interactive buckling of biaxially loaded elastic plate structures', *Ph.D. Thesis*, University of Waterloo, Ont., Canada, 1989.
18. R. Maaskant and J. Roorda, 'Mode jumping in biaxially compressed plates', *Int. J. Solid Struct.*, **29,** 1209–1220 (1992).
19. W. J. Supple, (ed.), *Coupled Buckling Modes of Structures, Structural Instability*, IPC Sci. Tech. Press, Guildford, 1973, pp. 28–53.
20. T. R. Graves Smith and S. Sridharan, 'A finite strip method for the post locally buckled analysis of plate structures', *Int. J. Mech. Sci.*, **20,** 833–842 (1978).
21. S. Sridharan and T. R. Graves Smith, 'Post-buckling analyses with finite strips', *J. Eng. Mech. Div. ASCE*, **107**(EM5), 869–888 (1981).
22. R. Benito and S. Sridharan, 'Interactive buckling analysis with finite strips', *Int. j. numer. methods. eng.*, **21,** 145–161, (1985).
23. R. Benito and S. Sridharan, 'Mode interaction in thin-walled structural members', *J. Struct. Mech. ASCE*, **12,** 517–542 (1985).
24. S. Sridharan and M. A. Ali, 'Interactive buckling in thin-walled beam-columns', *J. Eng. Mech.*, **111,** 1470–1486 (1985).
25. Sridharan and A. Ali, 'An improved interactive buckling analysis of thin-walled columns having doubly symmetric cross-sections', *Int. J. Solids Struct.*, **22,** 429–443 (1986).
26. S. Sridharan and M.-H. Peng 'Performance of axially compressed stiffened panels', *Int. J. Solids Struct.*, **25,** 879–899 (1987).
27. H. Mollmann and P. Goltermann, 'Interactive buckling in thin-walled beams, I. Theory', *Int. J. Solids Struct.*, **25,** 715–728 (1989).
28. R. Casciaro, G. Salerno and A. D. Lanzo, 'Finite element asymptotic analysis of slender elastic structures: a simple approach', *Int. j. numer. methods eng.*, **35,** 1397–1426 (1992).
29. W. T. Koiter, 'On the stability of elastic equilibrium', *Thesis*, Delft University of Technology, The Netherlands, English Translation NASA TTF-10833, 1967.
30. W. T. Koiter and M. Pignataro, 'A general theory for the interaction between local and overall buckling of stiffened panels', *Rep. 556*, Dep. Mech. Eng., Delft University of Tech., The Netherlands, 1976.
31. Z. Kolakowski, 'Mode interaction in thin-walled trapezoidal column under uniform compression', *Thin-Walled Struct.*, **5,** 329–342 (1987).
32. Z. Kolakowski, 'Some thoughts on mode interaction in thin-walled columns under uniform compression', *Thin-Walled Struct.*, **7,** 23–35 (1989).
33. Z. Kolakowski, 'Interactive buckling of thin-walled beam-columns with open and closed cross sections', *Thin-Walled Struct.*, **15,** 159–183 (1993).
34. F. Stoll, 'Analysis of non-linear response of compressive loaded stiffened panels', *First Joint Meeting SES-ASCE-ASME*, Charlottesville, VA, 6–9 June, 1993.
35. S. Sridharan and Starnes, 'Mode interaction in stiffened composite panels', *First Joint Meeting SES-ASCE-ASME*, Charlottesville, VA, 6–9 June, 1993.
36. J. G. A. Croll, and A. Walker, *Elements of Structural Stability*, McMillan, London, 1972.

37. S. T. Mau, and R. H. Gallagher, 'A finite element procedure for Non-linear prebuckling and initial postbuckling analysis, *NASA-CR-1936*, 1972.
38. R. H. Gallagher, 'Perturbation procedures in nonlinear finite element structural analysis, in *Lecture Notes in Mathematics*, Vol. 461, *Computational Mechanics*, Springer, Berlin, 1975, pp. 75–90.
39. O. C. Zienkiewicz and Taylor, *The Finite Element Method*, 4th edn, Vol. 2, McGraw Hill, London, 1991.
40. I. G. Raftoyiannis, 'Buckling mode interaction in FRP columns', *Ph.D. Dissertation*, West Virginia University, 1994.
41. J. N. Reddy, *Energy and Variational Methods in Applied Mechanics*, Wiley, New York, 1984.
42. E. J. Barbero, and R. Zinno, 'Analysis of laminated composite plates with three-dimensional layer-wise constant shear elements', *Int J. Eng. Anal. Des.*, **1**(1) (1994).
43. S. Ahmad, B. M. Irons and O. C. Zienkiewicz, 'Analysis of thick and thin shell structure by curved finite elements', *Int. j. numer. methods eng.*, **2**, 419–451 (1970).
44. E. J. Barbero, L. A. Godoy and S. Jones, 'Influence of bending extension coupling on buckling and postbuckling of composite columns', *Mechanics of Composite Materials and Structures*, to appear.
45. L. Godoy, E. J. Barbero and Raftoyiannis, 'Interactive buckling analysis of FRP columns', *J. Composite Mater.*, **29**, 591–613 (1995).